A Bending Test Protocol for Characterizing Mechanical Performance of Flexible Photovoltaics

Kenjiro Fukuda,[1,2] Lulu Sun[1], Baocai Du[2,3], Masahito Takakuwa[3,4], Jiachen Wang[5], Takao Someya[1,2,3], Lluis F. Marsal[6], Yinhua Zhou[7], Yiwang Chen[8], Hongzheng Chen[9], S. Ravi P. Silva[10], Derya Baran[11], Luigi A. Castriotta[12], Thomas M. Brown[12], Changduk Yang[13], Weiwei Li[14], Anita W.Y. Ho-Baillie[15], Thomas Österberg[16], Nitin P. Padture[17], Karen Forberich[18], Christoph J. Brabec[18,19], Osbel Almora[6]**

[1] *Thin-Film Device Laboratory, RIKEN, 2-1 Hirosawa, Wako, Saitama, 351-0198, Japan*

[2] *RIKEN Center for Emergent Matter Science (CEMS), 2-1 Hirosawa, Wako, Saitama, 351-0198, Japan*

[3] *Department of Electrical Engineering and Information Systems, The University of Tokyo, 7-3-1 Hongo, Bunkyo-ku, Tokyo 113−8656, Japan*

[4] *Institute of Engineering Innovation, Graduate School of Engineering, The University of Tokyo, 7-3-1 Hongo, Bunkyo-ku, Tokyo 113−8656, Japan*

[5] *Institute for Chemical and Bioengineering, Department of Chemistry and Applied Biosciences, ETH Zürich, Vladimir Prelog Weg 1, Zürich CH-8093, Switzerland*

[6] *Department of Electronic, Electrical and Automatic Engineering, Universitat Rovira i Virgili, Tarragona 43007, Spain*

[7] *Wuhan National Laboratory for Optoelectronics, Huazhong University of Science and Technology, Wuhan 430074, China*

[8] *College of Chemistry and Chemical Engineering/Institute of Polymers and Energy Chemistry (IPEC), Nanchang University, 999 Xuefu Avenue, Nanchang 330031, China*

[9] *State Key Laboratory of Silicon and Advanced Semiconductor Materials, International Research Center for X Polymers, Department of Polymer Science and Engineering, Zhejiang University, Hangzhou 310027, P. R. China.*

[10] *University of Surrey, Guildford, Surrey GU2 7XH, United Kingdom*

[11] *Material Science and Engineering Program (MSE), Physical Sciences and Engineering Division (PSE), King Abdullah University of Science and Technology, Thuwal 23955-6900, Kingdom of Saudi Arabia*

[12] *Centre for Hybrid and Organic Solar Energy, Electronic Engineering Department, University of Rome Tor Vergata, Via del Politecnico 1, 00118, Rome, Italy*

[13] *School of Energy and Chemical Engineering, Perovtronics Research Center, and Graduate School of Carbon Neutrality, Ulsan National Institute of Science and Technology (UNIST), 50 UNIST-gil, Ulju-gun, Ulsan, 44919 South Korea*

[14] *State Key Laboratory of Organic-Inorganic Composites, Beijing University of Chemical Technology, Beijing 100029, China*

[15] *School of Physics and Sydney Nano Institute, The University of Sydney, Sydney, NSW 2006, Australia*

[16] *Epishine AB, Attorpsgatan 2, 582 73 Linköping, Sweden*

[17] *School of Engineering, Brown University, Providence, RI 02912, USA*

[18] *Forschungszentrum Jülich GmbH, Helmholtz Institute Erlangen-Nürnberg for Renewable Energy (HI ERN), Dept. of High Throughput Methods in Photovoltaics, Immewahrstraße 2, 91058 Erlangen, Germany*

[19] *Institute of Materials for Electronics and Energy Technology (i-MEET), Department of Materials Science and Engineering, Friedrich-Alexander-Universität Erlangen-Nürnberg, Martensstraße 7, 91058 Erlangen, Germany*

* kenjiro.fukuda@riken.jp, osbel.almora@urv.cat

Keywords: Flexible photovoltaic devices; mechanical strain; bending radius; bending axis; performance stability

Abstract

Flexible photovoltaic (PV) devices represent a promising research field with potential for wearable, portable, indoor and internet-of-things applications. Significant progress has been made in recent years, with flexible emerging PVs reporting power conversion efficiency (*PCE*) over 24%. Yet, there is a need for a unifying protocol to assess PV performance, compare research results, and evaluate the state-of-the-art achievements in flexible PVs. In this perspective article, a protocol is presented for measuring *PCE* over 1,000 bending cycles under 1% strain. Moreover, several good practice guidelines are proposed including bending procedures, flexibility testing with and without encapsulation, and ambient conditions during testing (*e.g.*, temperature, humidity, illumination). Notably, the importance of uniform application of bending radius and the testing of parallel and perpendicular orientations of bending axis with respect to the direction of the electric current are emphasized. These recommendations aim to promote consistency in device comparison and allow for better reproducibility.

1. Introduction

Mechanical flexibility is an important property in emerging photovoltaic (ePV) devices[1] such as organic[2,3], dye-sensitized[4], perovskite[5–8], quantum dots[9–11], and CZTSe[12,13] solar cells from their inception.[14,15] Furthermore, it also has potential in conventional silicon-based photovoltaic (PV) devices. [1617] The flexibility and the lightweight nature achieved by using thin plastic substrates leads to potential applications for surface-based power generation on clothing,[18,19] lightweight aircraft,[20] power sources for soft robots,[21] curved X-ray detectors,[22] among others.[23,24] Recent research advances have significantly improved the mechanical robustness of ePV solar cells, enabling them to be rolled into cylindrical shapes without damage and even withstanding crumpling,[8,25,26] while also exhibiting stretchability.[27,28] Purposely, several review papers on flexibility/stretchability can be found in the literature.[14,15,17,23,29–31]

However, despite the widely recognized importance of flexibility, the evaluation of mechanical robustness in PV technologies could benefit from further consistency[32]. The current status is that each research group claims its own "superior flexibility" based on selectively chosen parameters, leading to subjective assessments. This practice not only hinders an objective comparison between results from different research groups/articles, but also raises doubts on the novelty and validity of each “flexibility progress” in the field. Given the established stability assessment for next-generation solar cells,[33] and standardization by the International Electrotechnical Commission (IEC),[34] a comparable protocol is needed to evaluate flexible PVs effectively.

Attempts to systematically analyze the data and compare the operational performance of flexible solar cells have recently been undertaken by the emerging PV initiative (https://emerging-pv.org/) and their yearly reports.[1] These platforms (an online database and a series of yearly review articles) track data and provide insights into the behavior of key parameters such as the power conversion efficiency (*PCE*), open-circuit voltage (V_{OC}), short-circuit current density (J_{SC}), and fill factor (*FF*) as a function of the device bandgap energy (E_g) for high-efficiency flexible devices. However, these cells are included based on their *PCE* values and the categorical property of flexibility, meaning that two flexible devices with the same efficiency but different bending properties cannot be distinguished. Therefore, there is currently a lack of qualitative classification and quantitative estimation of the flexibility of these devices.

Notably, the standardization report on flexible displays by the IEC[35] provides a comprehensive description of relevant parameters for four types of strains: bending, rolling, torsion, and tension. Among these test methods, bending is particularly common for assessing the performance of flexible PVs using the bending radius as main parameter. The evaluations/analyses relating to bending radius are reasonable for understanding how the cells/modules maintain their performance depending on the degree of bending and the number of bending cycles (N_{bc}). However, failure or device degradation is determined by the strain caused by bending the device, rather than just the bending radius alone. Therefore, reports solely focused

on bending radius overlook other critical parameters that determine strain during testing, such as structures, materials, and thicknesses of the devices. Therefore, a more comprehensive consideration of these parameters is necessary for accurate and meaningful comparisons among different flexible PV technologies.

Herein, a protocol is proposed for a versatile assessment of the mechanical robustness and operational performance of flexible PV devices. Our approach involves examining the influence of substrate thickness and compliance as quantified by Young's modulus on the magnitude of strain at a consistent bending radius. The paper discusses procedures that facilitate the evaluation and comparison of mechanical stability for small-area photovoltaic cells in terms of the *PCE*. Furthermore, the paper presents several protocols to enable the investigation of the effects of encapsulation and the assessment procedures for large-area modules.

2 Bending setups, loading orientation, strain and cycles

There are three main setups for applying cyclic bending strains. The first setup is using a rod having a specific radius (**Figure 1a**). If the film is tightly wrapped around the rod without loosening, the bending radius R will match the radius of the rod. However, there are several types of potential damage resulting from contact with the part facing the rod. For instance, scratches onto the substrate surface reducing the optical transmission; scratches to the functional device layers such as active layers and electrodes causing fatal damage to the photovoltaic performance and conductivity loss; and/or scratches onto the encapsulation layer causing degraded barrier properties. If the rod-contact damage is deemed to be minor, this is the preferred setup as it ensures uniform radius of bending over the entire device. Potential approaches to minimize the degradation include a lubricant being applied to the rod to inhibit mechanical wear of the samples

If the rod-contact damage is unacceptable, then the second setup could be used, which involves fixing the PV films to two stages; with one stage being fixed and the other movable (**Figure 1b**). As the distance between the two stages becomes shorter, bending stress is applied to the PV film fixed to the stages. Considering the shortest distance between two stages (L) and the moving distance of the movable stage (X), the bending diameter ($2R$) does not correspond to the length (L), as the bent film has a more complex form than a simple curved shape having one bending radius. With this setup, the bending radius must be measured from the side view of the film to confirm the whole device is bent with a constant bending radius. We suggest to take a photo/image from the lateral view to measure the actual bending radius applied to the device appropriately (as shown in Figure 1b).

Another alternative is the third setup which uses a foldable stage (without a rod), where the flexible PV film is fixed to the foldable stages (**Figure 1c**). When the stages become folded, the film is bent with the bending radius according to the distance between the two stages. For the second and third setups, the effects of contact deterioration can be minimized since the bendable area does not touch other objects. In contrast, when using a film with thin thickness and soft

material (such as silicon elastomer or normal polymer film with a Young's modulus of ~10^6 Pa and ~10^9 Pa, and thicknesses of several tens of μm and ≤ 10 μm, respectively), random deformation can occur rather than continuous deflection due to their low stiffness.

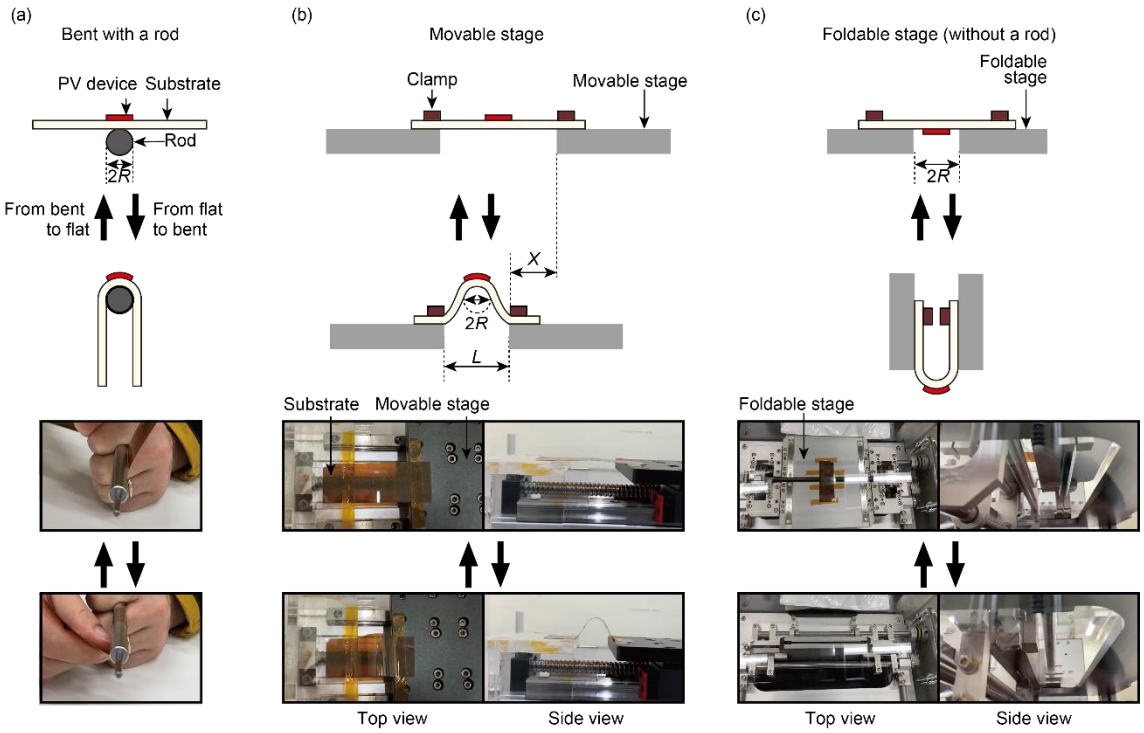

Figure 1: Bending setups. Schemed examples before and after the bending, and corresponding photos, (a) with a rod, (b) with a movable stage, and (c) with a foldable stage (without a rod). The vertical thick arrows indicate the cycles of bending (top: flat, bottom: bent).

The effective area of the device should be located in the center between the stages to apply the bending stress appropriately. This placement ensures that the strain is uniformly distributed across the device, preventing localized stress concentrations. In all cases, the effective bent region of specified radius *R* should be larger than that of the device. Given that the typical effective area of a small cell ranges from several mm^2 to ~1 cm^2, the strain may not be applied correctly to the cell when far smaller bending radii (than the device size) are used for cyclic bending tests. This hinders a fair comparison between the bending stability of a large-area module and single cells under similar conditions. Notably, for all setups in Figure 1, the device is bent outward (convex), but we can use the same setups and change the device location for the state in which the device is bent inward (concave).

Since the performance degradation depends on the bending-axis orientation with respect to the contact pads or busbars, the precise geometry of the device (including the design of contact pads or busbars) must be detailed, and the orientation of the bending axis should be clearly defined relative to direction of electric current extraction. A recommendation is given for testing in two

bending directions, parallel and perpendicular to a specific cell design, including contact pads or busbars, and regardless of the geometrical shape of the device (*e.g*. rectangular, square, circular). It is advised to perform these two experiments on separate samples to avoid cumulative damage, including a statistical analysis to rule out other non-mechanical instability contributions. For instance, when the bending axis is perpendicular to the electron flow direction, cracks are observed reaching the electrodes, causing interruptions in the current flow (as depicted in Figure 2a). This aspect is particularly crucial near the contacts where mechanical clamps are positioned.

The sensitivity to cell (rectangular) geometry is illustrated in Figure 2b and c. Samples with identical active areas but different contact regions may experience varying degrees of performance decline after stability testing. Conversely, when the bending axis aligns parallel to the electron flow, the preferential orientation of the cracks does not disrupt current flow (as shown in Figure 2d-f). This decrease of contact resistance with the parallel bending direction leads to improvement of device performance in the absence further parasitic effects. For instance, devices with sandwich electrode configurations in thin-film solar cells with transparent conducting oxides and large active area (with negligible border-effect photogeneration) should withstand the operational performance for more bending cycles in parallel than in perpendicular direction. Contrastingly, additional performance degradation may occur in the parallel bending direction after bending tests for samples with finger busbar electrodes, and depending on the size and geometry of the cell and the electrodes. Furthermore, such effects become more complex in panel configurations (as depicted in Figure 2g-j), where series connections may not only reduce the performance of multiple cells but also directly affect the metallic contacts between cells, and even disconnect them.

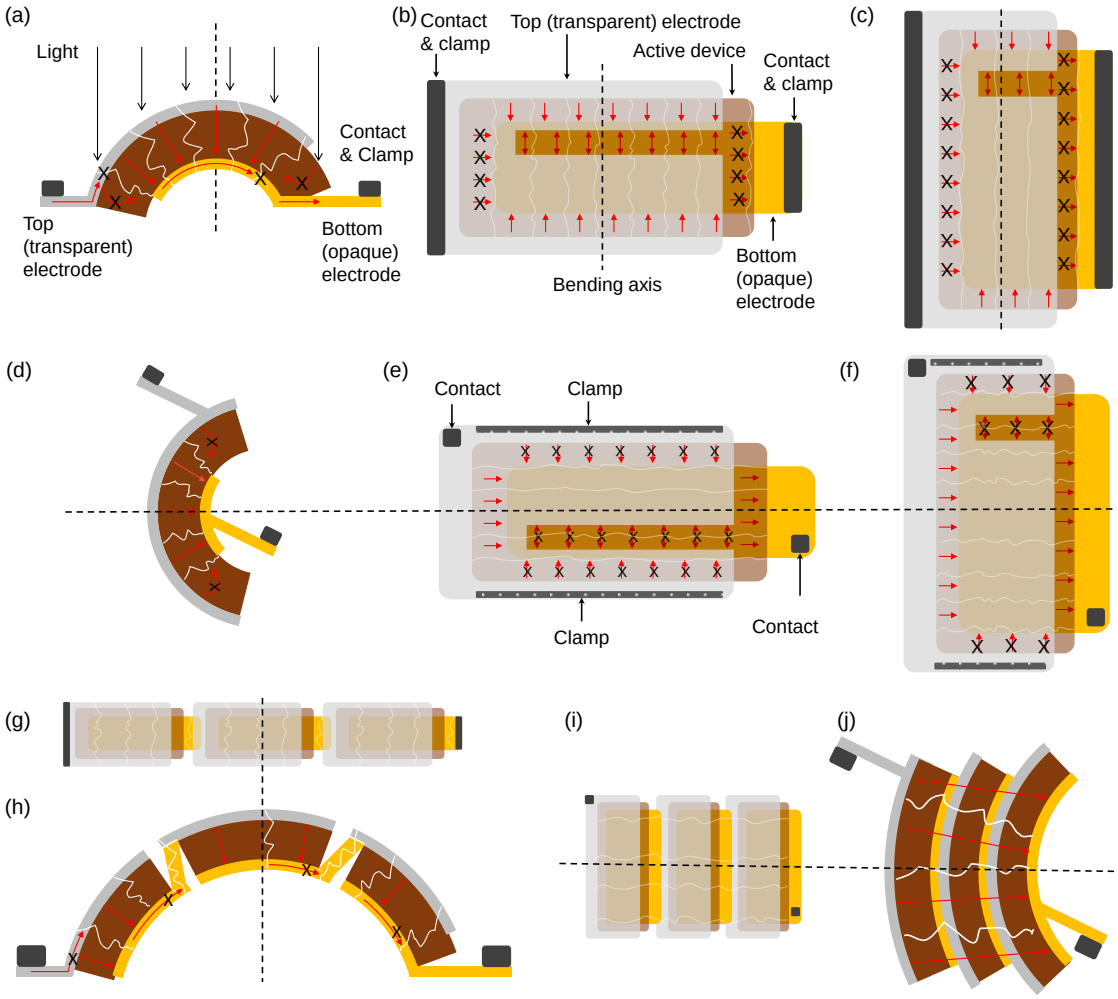

Figure 2: Sample bending. Schemed effects of different bending axis directions, sample geometries and connections. Top view (b, c, e, f, g, i) and cross sections (a, d, h, j) are shown for bending axes (dashed lines) perpendicular (a-c, g, h) and parallel (d-f, i, j) to the direction of electric current extraction (red arrows), in cells (a-f) and panels (g-j). The white serpentine lines indicate cracks and the crosses mark interruption of the electron flow. The subtracted area in the top electrodes resembles the case where the finger busbars are employed. Gray and yellow indicate top and bottom electrodes, respectively. Brown corresponds to the device, which may be composed by absorber and selective contact layers.

The applied strain during bending test depends on the thicknesses and Young's moduli of layers of the multi-stack structure of a flexible PVs. When using polymer films with Young's modulus in the order of 1 GPa and thicknesses exceeding 10 µm as substrates, the substrate thickness is much larger than the thicknesses of the other layers and the strain ε of the multi-layer structure can be calculated using the single-layer model [36,37]:

$$\varepsilon = {}^{t}/_{2R} \quad (1)$$

where t is the substrate thickness. However, in other cases, precise strain calculations require the multilayer model[23,3824,38]:

$$\varepsilon_{ML} = \frac{z-b}{R}, \quad (2)$$,

where z is the position along the thickness (z), and b is the neutral mechanical plane (zero-strain position) given by:

$$b = \frac{\sum_{i=1}^{n} E_i t_i \left[\sum_{j=1}^{i} t_j - \frac{t_i}{2}\right]}{\sum_{i=1}^{n} E_i t_i}, (3)$$

where E_i and t_i denote the Young's moduli and thicknesses of the individual layers. Accordingly, for determining the strain value, it is desirable to explicitly state the total thickness of a device and the thickness of each layer composing the stack.

Flexible PV that shows negligible degradation even when bent to an extremely small bending curvature radius (<1 mm) has been reported[25,26,39]. Therefore, assessing fatigue based on cyclic strains according to the number of cycles leads to a fairer comparison, rather than quasi-static stresses where slow and monotonically increasing stresses are applied to the device. Notably, tensile strain during bent state corresponds to outward bent devices, while inward bent devices present compressive strain. Specifying the strain type, tensile or compressive, is strongly recommended.

Appropriate strain values smaller than that of the crack-onset strain (COS) are to be considered during repeated bending tests of flexible PVs from stress-strain curves.[40,4137] A property of a functional material (*e.g.*, conductivity) rapidly deteriorates when a larger strain than that of the COS is applied, leading to device failure.[42] The COS value is typically obtained from the film via elastomer tests.[43] For example, indium-tin-oxide (ITO) and halide perovskites are brittle materials for ePVs, with reported COS values of ~ 0.6-1.5%.[37,44] and ~1.2%[45,46], respectively. In contrast, the polymers used in photoactive layers of organic solar cells have COS values ranging from a few percent to over 100%.[43] The current flow occurs vertically between top and bottom electrodes through active layers in the effective area region, whereas the flow occurs laterally along with each electrode in the contact pads or busbars region. The degradation intensity may depend on the direction in which the property of that material is measured, as we discussed in Figure 2. For example, cracks induced by bending could impede charge carriers in the lateral direction, but may have a less severe impact in the vertical direction.

In addition to COS, the Yield strain (ε_Y) indicating the limit of strain at which a material shows elastic deformation should also be considered. Otherwise, the N_{bc} for bending tests become too large to produce significant decrease of device performance. The values of both, the ε_Y and the COS of a film attached to an elastic and adhesive substrate, can be higher than those of the corresponding free-standing films[47–50]. Therefore, when using such elastomeric and adhesive substrates, it is recommended to evaluate the strain-stress curve for measuring ε_Y and COS in the most brittle material of the stack. Particularly, the use of a film with a multilayer structure (similar to the device structure) is recommended with a dumbbell or dog-bone shape[51]. If brittle materials are included, a strain value of 1% is usually estimated to be within the appropriate range.

Evaluating the mechanical stability of flexible PVs involves assessing changes in performance via repeated cycles between bent and flat states. Many reports adopt a range of approximately 10^3–10^4 cycles,[52–54] following established fatigue testing methods, commonly employed for the study of metals.[55] In the case of such high-strength materials, fatigue failure is classified into high- and low-cycle fatigue, with over or fewer than 10^4 cycles, in which a specific $\varepsilon < \varepsilon_Y$ and $\varepsilon_Y < \varepsilon <$COS is used, respectively.[40] While high-cycle fatigue entails minimal plastic deformation and operates within the elastic strain range, low-cycle fatigue involves repetitive plastic deformation. When the strain value is extremely small, high-cycle fatigue-like behavior is exhibited, and it is conceivable that performance deterioration hardly occurs at repeated strains of about 10^3–10^4 bending cycles. Strain values significantly lower than the yield strain (*e.g.*, 0.1% or less) may be insufficient for a N_{bc} as low as 10^3-10^4 and may have negligible impact on device performance. Therefore, a higher N_{bc} or larger strains are required in such cases. In addition, we recommend bending speed values ranging from 0.15 to 30 cycles/min. This agrees with the IEC standard for mechanical test methods of flexible display devices, which specifies the range of time for one bend and interval as between 0.5 s and 10 s.[35] Notably, 30 cycles/min corresponds to over 5.5 hours to obtain 10^4 cycles. Moreover, a large N_{bc} of more than 10^4 necessitates consideration of additional factors that may significantly contribute to degradation.

In summary, the recommendation is for the number of bending cycles $N_{\mathrm{bc}} = 10^3$, and a bending radius that gives a strain value of $\varepsilon = 1\%$, for which plastic deformation is expected to occurs, and thereby a decrease of performance can be observed. However, the suggested strain value is not applicable when testing a devices with $\varepsilon_Y, COS \gg 1\%$. This is particularly relevant for certain stretchable solar cells that may require additional cyclic stretching tests. Moreover, as the long-term storage and operational stability of flexible PVs improves over time, it may be advisable to increase the number of cycles to 10^4, or greater.

3. Encapsulation and environmental test conditions

Typical encapsulation systems consist of an adhesive and a permeation barrier layer completely adhering to the device substrate.[56–58] Then, the device is placed between the encapsulation layers (substrate and top/bottom encapsulation) (Figure 3) and the maximum strain occurs on the surface of the bottom or top encapsulation layer. Therefore, the device can be near the neutral strain position, which reduces the strain value applied to the device. Illustratively, Sekitani *et al*. have compared organic thin-film transistors (TFTs),[59] showing that a neutral-strain position reduces the failure radius from ~1 mm to ~0.5 mm, despite the materials and thicknesses of device and substrate are the same. The extreme small critical bending radii (10 μm or less) of recently reported ultra-thin ePVs also benefits mainly from this neutral strain position strategy.[8,25,39]

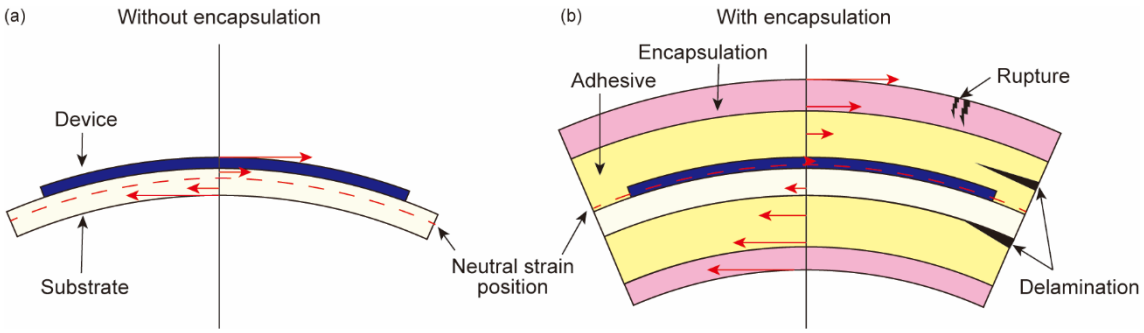

Figure 3: Encapsulation and bending. Strain distribution without (a) and with encapsulation (b). Red arrows represent strain vectors at each position. For the case without encapsulation, the maximum strain is applied to the surface of the device and the substrate, whereas for the case with encapsulation, the maximum strain is applied to the encapsulation layer and substrate. The strain applied to the device can be minimized by the addition of encapsulation, but the encapsulation layer can suffer from degradation itself (such as rupture and delamination).

Additionally, the use of an encapsulation layer can itself contribute to preventing device failure by suppressing local strains near pinholes/microcracks and interlayer delamination.[60] When an encapsulation layer is added to the device, the maximum strain occurs on the surface of the encapsulation film rather than on device surface. Therefore, greater attention must be more paid to the brittleness of the encapsulation layers (such as s silicon nitride or silicon oxide films) rather than the device layers. Rupture or interlayer delamination occur between the encapsulation and a device during repeated bending cycles, potentially resulting in a decline in gas barrier properties. Also, as the thickness of the adhesive layer increases, the adhesive layer also undergoes larger strain values. In such cases, some combinations of brittleness and thickness of UV-curable adhesives may lead to delamination between the device and the sealing film, or a decrease in sealing performance due to cracks in the adhesive layer. To assess the potential alteration in gas barrier properties of the encapsulation film, it is crucial to subject encapsulated devices to repeated bending stability tests under real ambient conditions, where the device is used (for most cases, ambient air conditions). In doing so, specifying the maximum strain expected to impact the encapsulation film enables a thorough evaluation under different conditions. Moreover, specifying the weight in terms of mass per photoactive area (kg cm^{-2}) is recommended, not only for all the samples but also specifically for those including encapsulation.

Other environment factors can also cause degradation in addition to that from the bending tests. For example, conducting more than 10^3 bending cycles, which can span several hours to complete the test, for unencapsulated samples, may lead to further degradation caused by extrinsic oxidation. Even encapsulated samples can degrade due to intrinsic unintended reactivity, phase separation, and/or diffusion of material species, which can be triggered by light, temperature, and electrical bias.[61,62] Therefore, it is essential to indicate the environment in which the cyclic bending test is conducted (e.g., ambient air or N_2). Comparing the bending stability under different

environments is fundamentally challenging. Therefore, it is recommended using the conditions listed in **Table 1**: first, unencapsulated devices in an inert atmosphere; second, unencapsulated device in ambient air; and third, encapsulated device in ambient air.

Further recommendations for the cyclic test in ambient air, according to the IEC standard for flexible displays, [35] include: temperature: 25 °C ± 3 °C; relative humidity (RH): 25 % to 85 %; and atmospheric pressure (AP): 86 kPa to 106 kPa. Moreover, a comparison with a device stored in the same environment (no bending strain experienced) is strongly recommended to discuss deterioration due to other parameters other than bending, as suggested by Zheng *et al*.[63] , This comparison is specifically recommended when testing at a high N_{bc}, when the speed of one cycle is very low, or with ultra-thin substrate/passivation technologies that can sacrifice barrier properties of water-oxygen to achieve minimized strain during bending. Furthermore, we recommend describing the change in PCE after bending cycles in either of the three bending test conditions listed above, providing both the measured *PCE* change and the difference in *PCE* change compared to samples that have been stored under the same conditions, but have not been subjected to mechanical strain.

Photo-instability is also a typical issue among rigid ePV devices. Consequently, it is recommended to perform the bending tests for analyzing mechanical stability (A and B in **Table 1**) in the dark and under open-circuit (OC) conditions. Therefore, the PCE of the sample should be measured before and after the stability test, under standard one sun illumination conditions. Ideally, these experiments should be designed to mainly characterize the effect of mechanical stress by minimizing other degradation factors and parameter change. Unfortunately, in most cases, only optical or visual information is accessible during these bending tests. As a result, the time-dependent evolution of the electrical properties is often unavailable, and the sample may fail before the completion of the test, precluding further assessment. Alternatively, a mechanical and operational stability test (C in **Table 1**) can also be performed under constant one-sun illumination intensity with continuous maximum power point (MPP) tracking.[61] In this case, the in-situ measurement of *J-V* curves is recommended after each bending cycle (or every conveniently small number of cycles), which in some cases complicates the already challenging characterization, such as in PSCs[64]. For instance, the *J-V* measurements must be in phase with the bending cycling in a way that it is performed while the sample is flat, to match the calibration for standard illumination intensity. This and the required wiring for electric biasing of the sample are acknowledged to hinder the implementation of method C in **Table 1**.

4. Conclusions

Significant progress has been made in flexible emerging PV devices over the last decade; however, a systematic protocol for characterizing mechanical stability and comparing device performance has been lacking in the literature. To address this gap, the importance of strain quantification over curvature radius has been emphasized, and several recommendations have been provided for best practices in mechanical stability tests. We highlight for a homogeneous distribution of bending

radius during the bending test, and the detailed description of the bending orientation and the exact geometry of the sample with respect to its contact and clamping points. Testing in both parallel and perpendicular orientations of the bending axis relative to the direction of electrical current is also recommended.

A protocol is presented for measuring the PCE before and after, or during, 1,000 bending cycles under 1% strain. **Table 2** summarizes the suggested protocols for bending cycle mechanical stability tests and a checklist recommendation is included in the supporting information. These protocols are applicable not only to mainstream emerging photovoltaics such as organic and perovskite devices, but also to any other flexible solar cells, including flexible quantum dot, nanocrystal, kesterite, and silicon cells. Furthermore, the aforementioned mechanical performance characterization protocols are recommended as an initial framework to foster progress in other flexible optoelectronic devices, such as photodetectors, light-emitting diodes, transistors, memristors, and supercapacitors.

Importantly, the bending tests are a primary metric for mechanical robustness, and the recommendations in this manuscript provide a fundamental starting point for the systematic characterization of mechanical device performance in PV cells. More detailed and in-depth studies may be necessary, and we acknowledge that stretchability, adhesion, and chemical inertness are crucial for long-term stability.

Acknowledgements

This study was supported by Japan Society for the Promotion of Science under Grants-in-Aid for Scientific Research (S) (No. JP22H04949). K.Fu. acknowledges the support from JST ASPIRE for Rising Scientists (JPMJAP2336). O.A. acknowledges the Juan de la Cierva Fellowship grant FJC2021-046887-I funded by MICIU/AEI/ 10.13039/501100011033 and by the European Union NextGenerationEU/PRTR. K.Fo. acknowledges support by the Helmholtz Association in the framework of the innovation platform “Solar TAP”. A H.-B is supported by the Australian Research Council (ARC) via Future Fellowship FT210100210. N.P.P. acknowledges the support from US DOE EERE SETO (DE-EE0009511). The authors thank Sixing Xiong of RIKEN (Japan) for his support with the photography of the bending setup.

Competing Interests

The authors declare no competing interests.

References

1. Almora, O. *et al.* Device Performance of Emerging Photovoltaic Materials (Version 4). *Adv. Energy. Mater.* **14**, 2303173 (2024).
2. Xiao, Z. *et al.* Ecofriendly Cellulose Substrate-Based Flexible Transparent Electrode for Flexible Organic Solar Cells with Efficiency Over 18%. *Solar RRL* **8**, 2400206 (2024).

3. Lu, X. *et al.* Increase in the efficiency and stability of large-area flexible organic photovoltaic modules via improved electrical contact. *Nat. Energy* **9**, 793–802 (2024).
4. Weerasinghe, H. C., Huang, F. & Cheng, Y.-B. Fabrication of flexible dye sensitized solar cells on plastic substrates. *Nano Energy* **2**, 174–189 (2013).
5. Cai, W. *et al.* Interfacial Engineering for Efficient Low-Temperature Flexible Perovskite Solar Cells. *Angew. Chem. Inte. Ed.* **62**, e202309398 (2023).
6. Xu, W. *et al.* Multifunctional entinostat enhances the mechanical robustness and efficiency of flexible perovskite solar cells and minimodules. *Nat. Photon.* **18**, 379–387 (2024).
7. Wu, Y. *et al.* Stereoscopic Polymer Network for Developing Mechanically Robust Flexible Perovskite Solar Cells with an Efficiency Approaching 25%. *Adv. Mater.* **36**, 2403531 (2024).
8. Hailegnaw, B. *et al.* Flexible quasi-2D perovskite solar cells with high specific power and improved stability for energy-autonomous drones. *Nat. Energy* **9**, 677–690 (2024).
9. Yang, W. *et al.* Overcoming Charge Confinement in Perovskite Nanocrystal Solar Cells. *Adv. Mater.* **35**, 2304533 (2023).
10. Hu, L. *et al.* Flexible and efficient perovskite quantum dot solar cells via hybrid interfacial architecture. *Nat. Commun.* **12**, 466 (2021).
11. Kramer, I. J. & Sargent, E. H. The architecture of colloidal quantum dot solar cells: Materials to devices. *Chem. Rev.* **114**, 863–882 (2014).
12. Xu, X. *et al.* 12.84% Efficiency Flexible Kesterite Solar Cells by Heterojunction Interface Regulation. *Adv. Energy Mater.* **13**, 2301701 (2023).
13. Deng, H. *et al.* Novel symmetrical bifacial flexible CZTSSe thin film solar cells for indoor photovoltaic applications. *Nat. Commun.* **12**, 3107 (2021).
14. Li, X. *et al.* Review and perspective of materials for flexible solar cells. *Mater. Rep.: Energy* **1**, 100001 (2021).
15. Dauzon, E. *et al.* Pushing the Limits of Flexibility and Stretchability of Solar Cells: A Review. *Adv. Mater.* **33**, 2101469 (2021).
16. Liu, W. *et al.* Flexible solar cells based on foldable silicon wafers with blunted edges. *Nature* **617**, 717–723 (2023).
17. Subudhi, P. & Punetha, D. Progress, challenges, and perspectives on polymer substrates for emerging flexible solar cells: A holistic panoramic review. *Prog. Phot. Res. Appl.* **31**, 753–789 (2023).
18. Jeong, E. G., Jeon, Y., Cho, S. H. & Choi, K. C. Textile-based washable polymer solar cells for optoelectronic modules: Toward self-powered smart clothing. *Energy Environ. Sci.* **12**, 1878–1889 (2019).
19. Wang, Z. *et al.* Self-sustaining personal all-day thermoregulatory clothing using only sunlight. *Science* **382**, 1291–1296 (2023)
20. Tu, Y. *et al.* Perovskite Solar Cells for Space Applications: Progress and Challenges. *Adv.*

Mater. **33**, 2006545 (2021)

21. Kakei, Y. *et al.* Integration of body-mounted ultrasoft organic solar cell on cyborg insects with intact mobility. *npj Flex. Electron.* **6**, 78 (2022).
22. Nanayakkara, M. P. A. *et al.* Molecular Weight Tuning of Organic Semiconductors for Curved Organic–Inorganic Hybrid X-Ray Detectors. *Adv. Sci.* **9**, 2101746 (2022).
23. Hu, Y. *et al.* Flexible Perovskite Solar Cells with High Power-Per-Weight: Progress, Application, and Perspectives. *ACS Energy Lett.* **6**, 2917–2943 (2021).
24. Fukuda, K., Yu, K. & Someya, T. The Future of Flexible Organic Solar Cells. *Adv. Energy Mater.* **10**, 2000765 (2020).
25. Lee, G. *et al.* Ultra-flexible perovskite solar cells with crumpling durability: toward a wearable power source. *Energy Environ. Sci.* **12**, 3182–3191 (2019.
26. Zheng, X. *et al.* Versatile organic photovoltaics with a power density of nearly 40 W g^{-1}. *Energy Environ. Sci.* **16**, 2284–2294 (2023).
27. Huang, J. *et al.* Intrinsically stretchable, semi-transparent organic photovoltaics with high efficiency and mechanical robustness *via* a full-solution process. *Energy Environ. Sci.* **16**, 1251–1263 (2023).
28. Lee, J. *et al.* Intrinsically Stretchable, Highly Efficient Organic Solar Cells Enabled by Polymer Donors Featuring Hydrogen-Bonding Spacers. *Adv. Mater.* **34**, 2207544 (2022).
29. Li, S., Li, Z., Wan, X. & Chen, Y. Recent progress in flexible organic solar cells. *eScience* **3**, 100085 (2023).
30. Hashemi, S. A., Ramakrishna, S. & Aberle, A. G. Recent progress in flexible–wearable solar cells for self-powered electronic devices. *Energy Environ. Sci.* **13**, 685–743 (2020).
31. Zhang, J., Zhang, W., Cheng, H.-M. & Silva, S. R. P. Critical review of recent progress of flexible perovskite solar cells. *Mater. Today* **39**, 66–88 (2020).
32. Dai, Z. & Padture, N. P. Challenges and opportunities for the mechanical reliability of metal halide perovskites and photovoltaics. *Nat. Energy* **8**, 1319–1327 (2023).
33. Khenkin, M. V. *et al.* Consensus statement for stability assessment and reporting for perovskite photovoltaics based on ISOS procedures. *Nat. Energy* **5**, 35–49 (2020).
34. International Electrotechnical Commission. Nanotechnology-reliability assessment - Part 2-1: Nano-enabled photovoltaic devices - stability test. **IEC TS 62876-2-1** (2018).
35. International Electrotechnical Commission. Flexible display devices-Part 6-1: Mechanical test methods-Deformation tests. *Flexible display devices-Part 6-1: Mechanical test methods-Deformation tests.* **IEC 62715-6-1** (2018).
36. Sekitani, T. *et al.* Bending experiment on pentacene field-effect transistors on plastic films. *Appl. Phys. Lett.* **86**, 073511 (2005).
37. Leterrier, Y. Mechanics of curvature and strain in flexible organic electronic devices. in *Handbook of Flexible Organic Electronics: Materials, Manufacturing and Applications* 3–36 (Elsevier Inc., 2015). doi:10.1016/B978-1-78242-035-4.00001-4.

38. Kim, D. H. *et al.* Stretchable and foldable silicon integrated circuits. *Science* **320**, 507–511 (2008).
39. Kaltenbrunner, M. *et al.* Ultrathin and lightweight organic solar cells with high flexibility. *Nat Commun* **3**, 770 (2012).
40. Yan, C., Qin, J., Wang, Y., Li, G. & Cheng, P. Emerging Strategies toward Mechanically Robust Organic Photovoltaics: Focus on Active Layer. *Adv Energy Mater* **12**, 2201087 (2022).
41. Tu, Q., Kim, D., Shyikh, M. & Kanatzidis, M. G. Mechanics-coupled stability of metal-halide perovskites. *Matter* **4**, 2765–2809 (2021).
42. Méndez-Hernández, J. M., Hernández-Pérez, A., Oviedo-Mendoza, M. & Hernández-Rodríguez, E. Effects of mechanical deformations on P3HT:PCBM layers for flexible solar cells. *Mechanics of Materials* **154**, 103708 (2021).
43. Balar, N. & O'Connor, B. T. Correlating Crack Onset Strain and Cohesive Fracture Energy in Polymer Semiconductor Films. *Macromolecules* **50**, 8611–8618 (2017).
44. Hengst, C. *et al.* Mechanical Properties of ZTO, ITO, and a-Si:H Multilayer Films for Flexible Thin Film Solar Cells. *Materials* **10**, 245 (2017).
45. Yadavalli, S. K., Dai, Z., Zhou, H., Zhou, Y. & Padture, N. P. Facile healing of cracks in organic–inorganic halide perovskite thin films. *Acta Mater.* **187**, 112–121 (2020).
46. Ahn, S. M. *et al.* Nanomechanical Approach for Flexibility of Organic-Inorganic Hybrid Perovskite Solar Cells. *Nano Lett.* **19**, 3707–3715 (2019).
47. Wang, J. *et al.* Intrinsically stretchable organic photovoltaics by redistributing strain to PEDOT:PSS with enhanced stretchability and interfacial adhesion. *Nat. Commun.* **15**, 4902 (2024).
48. Lu, N., Wang, X., Suo, Z. & Vlassak, J. Metal films on polymer substrates stretched beyond 50%. *Appl. Phys. Lett.* **91**, 221909 (2007).
49. Hamasha, M. M., Alzoubi, K. & Lu, S. Behavior of sputtered indium-tin-oxide thin film on poly-ethylene terephthalate substrate under stretching. *J. Display Technol*. **7**, 426–433 (2011).
50. Root, S. E., Savagatrup, S., Printz, A. D., Rodriquez, D. & Lipomi, D. J. Mechanical Properties of Organic Semiconductors for Stretchable, Highly Flexible, and Mechanically Robust Electronics. *Chem. Rev.* 117 6467–6499 (2017).
51. Noh, J. *et al.* Intrinsically Stretchable Organic Solar Cells with Efficiencies of over 11%. *ACS Energy Lett.* **6**, 2512–2518 (2021).
52. Chen, X. *et al.* Realizing Ultrahigh Mechanical Flexibility and >15% Efficiency of Flexible Organic Solar Cells via a "Welding" Flexible Transparent Electrode. *Adv. Mater.* **32**, 1908478 (2020).
53. Dong, Q. *et al.* Flexible perovskite solar cells with simultaneously improved efficiency, operational stability, and mechanical reliability. *Joule* **5**, 1587–1601 (2021).

54. Dai, Z. *et al.* Dual-Interface-Reinforced Flexible Perovskite Solar Cells for Enhanced Performance and Mechanical Reliability. *Adv. Mater.* **34**, (2022).
55. Suresh, S. *Fatigue of Materials*. (Cambridge University Press, 1998). doi:10.1017/CBO9780511806575.
56. Ahmad, T., Dasgupta, S., Almosni, S., Dudkowiak, A. & Wojciechowski, K. Encapsulation Protocol for Flexible Perovskite Solar Cells Enabling Stability in Accelerated Aging Tests. *Energy Environ. Mater.* **6**, e12434 (2023).
57. Sutherland, L. J., Weerasinghe, H. C. & Simon, G. P. A Review on Emerging Barrier Materials and Encapsulation Strategies for Flexible Perovskite and Organic Photovoltaics. *Adv. Energy Mater.* **11**, 2101383 (2021).
58. Castro-Hermosa, S., Top, M., Dagar, J., Fahlteich, J. & Brown, T. M. Quantifying Performance of Permeation Barrier—Encapsulation Systems for Flexible and Glass-Based Electronics and Their Application to Perovskite Solar Cells. *Adv. Electron. Mater.* **5**, (2019).
59. Sekitani, T. *et al.* Ultraflexible organic field-effect transistors embedded at a neutral strain position. *Appl. Phys. Lett.* **87**, 173502 (2005).
60. Sawyer, E. J. *et al.* Large increase in stretchability of organic electronic materials by encapsulation. *Extreme Mech. Lett.* **8**, 78–87 (2016).
61. Rakocevic, L. *et al.* Reliable Performance Comparison of Perovskite Solar Cells Using Optimized Maximum Power Point Tracking. *Solar RRL* **3**, 1800287 (2019).
62. Wei, J. *et al.* Mechanisms and Suppression of Photoinduced Degradation in Perovskite Solar Cells. *Adv. Energy Mater.* **11**, 2002326 (2021).
63. Zheng, X. *et al.* High-Efficiency ITO-Free Organic Photovoltaics with Superior Flexibility and Upscalability. *Adv. Mater.* **34**, 2200044 (2022).
64. Jeong, S. H. *et al.* Characterizing the Efficiency of Perovskite Solar Cells and Light-Emitting Diodes. *Joule* 4 1206–1235 (2020).

Tables

Table 1. Environmental conditions suggested for bending cycle testing

Test Focus	Encapsulation	Environment	Biasing	Illumination	Further conditions
A: Unencapsulated device in inert atmosphere	No	Inert (e.g., a N_2-filled chamber)	OC	Dark	25 °C; 25-85 % RH; 86-106 kPa AP
B: Unencapsulated device in ambient air	No	Ambient air	OC	Dark	
C: Encapsulated device in ambient air	Yes	Ambient air	OC/MPP	Dark/1 sun (AM1.5G)	

Table 2. Recommended description of characterization protocol for bending cycle tests of flexible PV devices. The asterisk indicates the mandatory parameters to be specified in reports.

Classification/description	Parameter	Protocol details/comments
Device characteristics	Substrate thickness (t_s)*	Must be specified.
	Device thickness (t_d)	Recommended to specify effective average cross-section distance between electrodes.
	Each layer thickness	Recommended to be specified.
	Encapsulation*	Must be specified and described when present, including encapsulation (barrier layer and adhesive layer) thickness.
	Weight per photoactive area	Recommended to be specified in units of kg cm^{-2}
Environmental conditions	Atmosphere*	Must be specified (air or N_2-filed glove box). In the case of air, RH = 55% ± 15% recommended.
	Temperature*	Must be specified; 25°C recommended.
	Illumination*	Must specify dark, or illumination intensity and spectrum. In the case of illumination, standard 100 mW cm^{-2} AM1.5G spectrum is recommended.
	Atmospheric pressure	Specification encouraged; 96 kPa ± 10 kPa is recommended.
	Biasing*	Must specify open-circuit, short-circuit, constant bias, or MPP tracking. Open-circuit and MPP tracking are recommended, for dark and illuminated tests, respectively.
Bending conditions	Bending strain type/direction*	Must specify tensile or compressive strain depending on whether the device is in the outer or inner bending surface of the substrate, respectively.
	Bending radius*	Must be specified. The recommended value is that corresponding to the strain of ~1%.
	Suggested number of bending cycles*	Must be specified; 1,000 cycles recommended.
	Cycling speed or duration for one cycle	Specification encouraged; 0.15-30 cycles/min recommended.
	Bending axis orientation*	Must include graphic description of the bending axis direction, specifying the position of the electrodes and the exact geometry of the sample, including the contacts or busbars. Testing of both parallel and perpendicular orientations of the bending axis with respect to the direction of electric current flow is encouraged.
Strain calculation	With simple model	Mostly accepted

	with multi-stack model	Exceptional case for simple model cannot be applied (soft/thin substrate). Young's modulus can be referred from references.
Performance presentation	*PCE**	Must specify the initial and final PCE values under standard conditions before and after the mechanical bending test. In situ *PCE* as a function of cycle number encouraged.
	J_{SC}, *FF*, V_{oc}	Recommended to be measured and presented including the *J-V* curves and further performance parameters, before, during and after the bending test.
	External quantum efficiency (*EQE*)	Encouraged to be measured and presented before and after the bending test.

*Strongly recommended to state in the article